VOLUME 113, NUMBER 8
APRIL 10, 1991

JOURNAL
OF THE
AMERICAN
CHEMICAL
SOCIETY

Scanning Tunneling Microscopy of Ethanethiolate and *n*-Octadecanethiolate Monolayers Spontaneously Adsorbed at Gold Surfaces

Cindra A. Widrig,† Carla A. Alves, and Marc D. Porter*

Contribution from the Ames Laboratory-U.S. Department of Energy and Department of Chemistry, Iowa State University, Ames, Iowa 50011. *Received November 5, 1990*

Abstract: Monolayer films from ethanethiol (ET) and *n*-octadecanethiol (OT) spontaneously adsorbed onto epitaxially grown Au(111) films on mica were examined by scanning tunneling microscopy (STM). The resulting atomically resolved images are the first reported for gold-adsorbed organothiolate molecules and reveal the packing arrangement of the overlayer. Tunneling is presumed to occur between the microscope tip and the gold-bound sulfur of the *n*-alkanethiolate head group. For both the ET and OT monolayers, an image that corresponds to a hexagonally packed array of adsorbates with respective nearest-neighbor and next-nearest-neighbor spacings of 0.50 ± 0.02 and 0.87 ± 0.04 nm was observed. This packing agrees well with the $(\sqrt{3} \times \sqrt{3})R30°$ structure determined for long-chain *n*-alkanethiolate monolayers on Au(111) in recent helium diffraction[1] and electron diffraction[2] studies. Furthermore, images with the above spacings were found to exhibit continuity over areas from a few square nanometers up to about 600 nm^2, indicating the potential utility of STM for probing both the short- and long-range order of organic monolayer films. Structural interpretations of these images are presented and examined within the context of molecular level descriptions that have been recently developed from macroscopic characterization studies of these monolayers.

Introduction

Spontaneously adsorbed monolayer films of *n*-alkanethiolates[3] and their functionalized analogues have been extensively examined as model molecular systems for elucidating structure–reactivity relationships at metal–liquid interfaces.[1-6] As a result of such efforts, details concerning the macroscopic (average) structure, electronic properties, surface free energy, and imperfections of these layers are beginning to emerge. To utilize these results fully, however, it is also necessary to possess a microscopic understanding of the monolayer structure, including descriptions of the short- and long-range packing arrangement within the film. The relatively new technique of scanning tunneling microscopy (STM) provides the real-space atomic resolution required to obtain such information[7] at both organic[8] and inorganic[9] adsorbate layers. In this paper, we show that the application of STM to ethanethiolate- and *n*-octadecanethiolate-coated gold surfaces reveals the two-dimensional structure of the adsorbate.

In the following sections, we present and discuss the first STM images obtained for ethanethiolate (ET) and *n*-octadecanethiolate

* Author to whom correspondence should be addressed.
† Present address: Department of Chemistry and Biochemistry, Utah State University, Logan, UT 84322.

(1) Chidsey, C. E. D.; Liu, G.-Y.; Rowntree, P.; Scoles, G. *J. Chem. Phys.* **1989**, *91* (7), 4421–4423.
(2) (a) Strong, L.; Whitesides, G. M. *Langmuir* **1988**, *4*, 546–558. (b) For additional details: Chidsey, C. E. D.; Loiacono, D. N. *Langmuir* **1990**, *6*, 682–691.
(3) Evidence that these monolayers form as an *n*-alkanethiolate at the Au surface is given in: Widrig, C. A.; Chung, C.; Porter, M. D. *J. Electroanal. Chem.*, in press.
(4) Examples concerning organosulfur monolayers at Au include: (a) Nuzzo, R. G.; Allara, D. L. *J. Am. Chem. Soc.* **1983**, *105*, 4481–4483. (b) Li, T.-T.; Weaver, M. J. *J. Am. Chem. Soc.* **1984**, *106*, 6107–6108. (c) Nuzzo, R. G.; Zegarski, B. R.; Dubois, L. H. *J. Am. Chem. Soc.* **1987**, *109*, 733–740. (d) Porter, M. D.; Bright, T. B.; Allara, D. L.; Chidsey, C. E. D. *J. Am. Chem. Soc.* **1987**, *109*, 3559–3568. (e) Sabatani, E.; Rubinstein, I. *J. Phys. Chem.* **1987**, *91*, 6663–6669. (f) Bain, C. D.; Troughton, E. B.; Tao, Y.-T.; Evall, J.; Whitesides, G. M.; Nuzzo, R. G. *J. Am. Chem. Soc.* **1989**, *111*, 321–335. (g) Finklea, H. O.; Snider, D. A.; Fedyk, J. *Langmuir* **1990**, *6*, 371–376. (h) Dubois, L. H.; Zegarski, B. R.; Nuzzo, R. G. *J. Am. Chem. Soc.* **1990**, *112*, 570–579. (i) Nuzzo, R. G.; Dubois, L. H.; Allara, D. L. *J. Am. Chem. Soc.* **1990**, *112*, 558–569. (j) DeLong, H. C.; Buttry, D. A. *Langmuir* **1990**, *6*, 1319–1322.

0002-7863/91/1513-2805$02.50/0

(OT) monolayers spontaneously adsorbed on epitaxially grown Au(111) films. As discussed, we believe our images result from electrons tunneling between the microscope tip and the sample surface through the gold-bound sulfur of the *n*-alkanethiolate head group. For both ET and OT, an image that corresponds to a hexagonally packed adsorbate overlayer with respective nearest-neighbor and next-nearest-neighbor spacings of 0.50 (±0.02) and 0.87 (±0.04) nm was observed. The two-dimensional arrangement suggests that the surface is covered predominantly with a $(\sqrt{3} \times \sqrt{3})R30°$ overlayer on an underlying Au(111) lattice. This arrangement agrees with that reported by helium[1] and transmission electron[2] diffraction studies. In addition, images with the above spacings were found to exhibit continuity over areas of a few square nanometers up to about 600 nm^2. Such images suggest that STM can provide important evidence regarding the size and distribution of ordered domains within these monolayers. A structural interpretation of the images is presented and examined in the context of the molecular level descriptions that have been developed from recent studies with various macroscopic characterization techniques.[1,2,4]

Experimental Section

Monolayer Preparation. Gold substrates with a predominant (111) texture were prepared by the epitaxial growth of 200-nm gold films onto freshly cleaved mica sheets.[10,11] The mica sheets were nominally 1 in. by $^1/_2$ in. The deposition was carried out by resistive evaporation in a cryogenically pumped Edwards 306A vacuum chamber (West Sussex, England) at a pressure of $\sim 2 \times 10^{-6}$ Torr. Immediately prior to deposition, the mica was heated in vacuum at 200–300 °C for ~1 h. Gold was deposited onto the heated mica at a rate of 0.3–0.7 nm/s. Subsequently, the substrates were allowed to cool radiatively to below 70 °C, removed from the vacuum chamber, and immersed immediately in 1 mM ethanolic solutions of ET or OT to form the monolayers.[4b] The substrates were left in solution for 2–24 h, immersed, and rinsed thoroughly with ethanol. Variation of the immersion time did not observably affect the resulting images. These monolayers are structurally comparable to those prepared at Au films deposited at polished silicon wafers, as determined by infrared reflection spectroscopic, contact angle, and electrochemical capacitance measurements.[3] The ET was used as received (Aldrich); OT (Aldrich) was recrystallized twice from methanol.

Instrumentation. All images were acquired with a Digital Instruments Nanoscope II STM (Santa Barbara, CA). The instrument was equipped with a 450 nm × 450 nm scanning head and was operated in the laboratory ambient. With this instrument, the images are displayed as though the tip moves from right to left across the computer monitor; the figures in this paper maintain this presentation.

Images examining large (0.02–0.20 μm^2) sections of the sample were recorded under conditions for constant current (the "height" mode of the Nanoscope II). In this mode, a preselected tunneling current between the tip and sample is maintained via a feedback loop to a piezoelectric tube that adjusts the vertical position of the tip. The adjustments to maintain a constant tunneling current are recorded as the tip is rastered over the sample surface. Typical tunneling currents and bias voltages used for these images were 3 nA and +80 mV, respectively, with the sign of the bias voltage given with respect to the grounded substrate. The tips used for these large scans were fabricated from 0.010 in. diameter tungsten wire cut diagonally with wire cutters.

For atomically resolved images, conditions for constant height imaging were found more useful (the "current" mode of the Nanoscope II). In this mode, the vertical position of the tip is held constant with variations in the tunneling current recorded as the tip moves across the sample surface. Images were obtained under a range of bias voltages (−200 to +200 mV) and tunneling currents (1–10 nA). The tips used for the atomically resolved images were fabricated by etching electrolytically a 0.010 in. diameter tungsten wire in a solution of 1 M KOH.[12] Only those tips that readily provided well-defined images of highly ordered pyrolytic graphite (HOPG) were used. The lateral distances in these images were determined by using HOPG for calibration.

Results and Discussion

To develop a basis for the discussion of our results, we first describe the various control experiments performed to verify that our STM images result from the presence of the monolayer. We next present images for our uncoated Au films, which reveal both the topography and predominant (111) crystallinity of the surface. The latter images serve as a reference for the presentation and discussion of the images of the spontaneously adsorbed monolayers of ET and OT. We conclude with a structural assessment of these images in the context of molecular level descriptions that have been developed from various macroscopic characterization techniques and a brief discussion of a possible mechanism that gives rise to these images.

1. Reproducibility of Imaging *n*-Alkanethiolates on Au with STM. To date, the tunneling conditions that consistently allow the observation of a well-defined image have been difficult to define fully. We attribute this primarily to preparative variability of the shape and/or composition of the tip. "Good" and "bad" tips were distinguished solely on the basis of their ability or inability to resolve atomic structure at HOPG. Once constructed, a good tip was often used repeatedly. Also, images recorded upon initial engagement of a good tip at the sample surface frequently show no evidence of recognizable surface structure; it is only with time, displacement of the tip, and/or variation of the tunneling conditions that periodic features at an atomic level become apparent. It is usual that once a structure is observed, successive scans over the same area reproduce the image for several minutes up to an hour, after which time the image gradually or suddenly disappears. Moderate variation in the tunneling current (0.5–10 nA) and bias voltage (±20 to ±300 mV) during the time that the image is "in focus" usually does not lead to loss of the image. Instabilities in the tip shape or composition may cause this focusing and loss of atomically resolved images.[8n,9e,11]

Because of the above difficulties, we cannot directly conclude that our images are representative of the structure across the entire

(5) (a) Sandroff, C. J.; Garoff, S.; Leung, K. P. *Chem. Phys. Lett.* **1983**, *96*, 547–551. (b) Joo, T. H.; Kim, K.; Kim, M. S. *J. Phys. Chem.* **1986**, *90*, 5816–5819. (c) Blackman, L. C. F.; Dewar, M. J. S.; Hampson, H. *J. Appl. Chem.* **1957**, *7*, 160–171. (d) Prince, N. P.; Seymour, D. L. Woodruff, D. P.; Jones, R. G.; Walter, W. *Surf. Sci.* **1989**, *215*, 566–576. (e) Sobocinski, R. L.; Bryant, M. A.; Pemberton, J. E. *J. Am. Chem. Soc.* **1990**, *112*, 6177–6183. (f) Walczak, M. M.; Chung, C.; Stole, S. M.; Widrig, C. A.; Porter, M. D. *J. Am. Chem. Soc.*, in press.

(6) For additional leading references see: Whitesides, G. M.; Laibinis, P. E. *Langmuir* **1990**, *6*, 87–96.

(7) Binnig, G.; Rohrer, H. *Surf. Sci.* **1983**, *126*, 236–244.

(8) See, for example: (a) Feng, L.; Hu, C. Z.; Andrade, J. D. *J. Microsc.* **1988**, *152* (3), 811–816. (b) Hubacek, J. S.; Brockenbrough, R. T.; Gammie, G.; Skala, S. L.; Lyding, J. W.; Latten, J. L.; Shapley, J. R. *J. Microsc.* **1988**, *152* (1), 221–227. (c) Braun, H. G.; Fuchs, H.; Shrepp, W. *Thin Solid Films* **1988**, *159*, 301–314. (d) Lang, C. A.; Horber, J. K. H.; Hansch, T. W.; Heckl, W. M.; Mohwald, H. *J. Vac. Sci. Technol. A* **1988**, *6* (2), 368–370. (e) Eng, L.; Hidber, H.-R.; Rosenthaler, L.; Staufer, U.; Wiesendanger, R.; Guntherodt, H.-J.; Tamm, L. *J. Vac. Sci. Technol. A* **1988**, *6* (2), 358–359. (f) Smith, D. P. E.; Horber, H.; Gerber, Ch.; Binnig, G. *Science* **1989**, *245*, 43–45. (g) Smith, D. P. E.; Horber, J. K. H.; Binnig, G.; Nejoh, H. *Nature* **1990**, *344*, 641–644. (h) Foster, J. S.; Frommer, J. E. *Nature* **1988**, *333*, 542–545. (i) Smith, D. P. E.; Bryant, A.; Quate, C. F.; Rabe, J. P.; Gerber, Ch.; Swalen, J. P. *Proc. Natl. Acad. Sci. U.S.A.* **1987**, *84*, 969–972. (j) Horber, J. K. H.; Lang, C. A.; Hansch, T. W.; Heckl, W. M.; Mohwald, H. *Chem. Phys. Lett.* **1988**, *145*, 151–158. (k) Wu, X.-L.; Lieber, C. M. *J. Phys. Chem.* **1988**, *92*, 5556–5557. (l) Rabe, J. P.; Sano, M.; Batchelder, D.; Kalatchev, A. A. *J. Microsc.* **1988**, *152* (2), 573–583. (m) Moller, R.; Cohen, R. Esslinger, A.; Koslowski, B. *J. Vac. Sci. Technol. A* **1990**, *8* (1), 659–660. (n) Ohtani, H.; Wilson, R. J.; Chiang, S.; Mate, C. M. *Phys. Rev. Lett.* **1988**, *60* (23), 2398–2401. (o) McMaster, T. J.; Carr, H.; Miles, M. J.; Cairns, P.; Morris, V. J. *J. Vac. Sci. Technol. A* **1990**, *8* (1), 648–651. (p) Beebe, T. P.; Wilson, T. E.; Ogletree, D. F.; Katz, J. E.; Balhorn, R.; Salmeron, M. B.; Siekhaus, W. J. *Science* **1989**, *243*, 370–372. (q) Hameroff, S.; Simic-Krstic, Y.; Vernetti, L.; Lee, Y. C.; Sarid, D.; Wiedmann, J.; Elings, V.; Kjoller, K.; McCuskey, R. *J. Vac. Sci. Technol. A* **1990**, *8* (1), 687–691. (r) Sotobayashi, H.; Schilling, T.; Tesche, B. *Langmuir* **1990**, *6*, 1246–1250.

(9) See, for example: (a) Schardt, B. C.; Yau, S.-L.; Rinaldi, F. *Science* **1989**, *243*, 1050–1053. (b) Ogletree, D. F.; Ocal, C.; Marchon, B.; Somorjai, G. A.; Salmeron, M.; Beebe, T.; Siekhaus, W. *J. Vac. Sci. Technol. A* **1990**, *8* (1), 297–301. (c) Marchon, B.; Ogletree, D. F.; Bussell, M. E.; Somorjai, G. A.; Salmeron, M.; Siekhaus, W. *J. Microsc.* **1988**, *152* (2), 427–439. (d) Tokumoto, H.; Miki, K.; Murakami, H.; Bando, H.; Ono, M.; Kajimura, K. *J. Vac. Sci. Technol. A* **1990**, *8* (1), 255–258. (e) Avouris, Ph.; Wolkow, R. *Phys. Rev. B* **1989**, *39* (8), 5091–5100.

(10) Chidsey, C. E. D.; Loiacono, D. N.; Sleator, T.; Nakahara, S. *Surf. Sci.* **1988**, *200*, 45–66.

(11) (a) Hallmark, V. M.; Chiang, S.; Rabolt, J. F.; Swalen, J. D.; Wilson, R. J. *Phys. Rev. Lett.* **1987**, *59* (25), 2879–2882. (b) Emch, R.; Nogami, J.; Dovek, M. M.; Lang, C. A.; Quate, C. F. *J. Appl. Phys.* **1989**, *65*, 79–84.

(12) Yau, S.-L.; Vitus, C. M.; Schardt, B. C. *J. Am. Chem. Soc.* **1990**, *112*, 3677–3679.

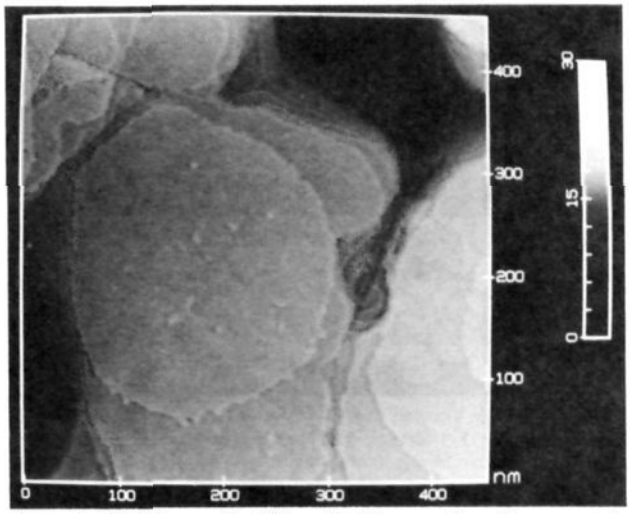

Figure 1. STM image of a 450 nm × 450 nm section of an uncoated epitaxially grown Au film on mica. The image was recorded in the constant current mode, without filtering, using a bias voltage of +80 mV and a tunneling current of 3 nA. The light to dark color scale (z scale) is 0–30 nm.

surface of the sample. Such an extrapolation is also complicated because the actual surface area examined is very small ($\sim 10^{-13}$–10^{-12} cm^2). We are confident, however, that the images described below result from the presence of the monolayer and extend in some cases over areas as large as 600 nm^2. Several control experiments support our contention.[13] First, each of the images reported has been observed on several ($\geq$20) samples of each adsorbate. Second, we have yet to observe images comparable to those of the thiol adsorbate at our uncoated Au or at uncoated Au exposed to neat ethanol. Third, preliminary experiments with monolayers containing long fluorocarbon chains [e.g., $CF_3(CF_2)_7(CH_2)_2SH$] yield images with a larger nearest-neighbor separation than found for the ET and OT layers. The latter observation is consistent with the packing limitations of the $\sim$5.6 Å diameter of perfluoromethylene chains[2b] as opposed to that of the $\sim$4.2 Å diameter of methylene chains.[14] Together, these results indicate that our images result from the presence of the sulfur-bound alkanethiolate.

2. STM Characterization of Uncoated Au Films on Mica. Figure 1 is a STM image of a 450 nm × 450 nm section of a thin gold film that was epitaxially deposited onto freshly cleaved mica. This image was recorded by using the constant current mode. This and all other images shown are gray-scale images in which the lighter areas correspond to higher regions of the surface and the darker areas to lower regions of the surface. The color scale for the height range of each figure is shown to the right of the image. As previously observed,[10,11] the image in Figure 1 shows the gold film to comprise atomically flat crystallites that are a few hundred nanometers in diameter and are separated by grain boundaries of varied width. Profiles of the grain boundaries are difficult to assess because of possible tunneling between the side of the tip and the sides of the crystallites. The image shown was recorded immediately after removal of the sample from the evaporator, though continued storage of the bare substrate in the laboratory ambient does not affect the images at a noticeable level.

An atomically resolved 2.3 nm × 2.3 nm image of an uncoated gold substrate is shown in Figure 2A. Hexagonal arrays of bright spots are evident throughout the image. This is the only periodic feature on our uncoated Au substrates that we have observed to date, having examined more than 30 samples. Figure 2B is a

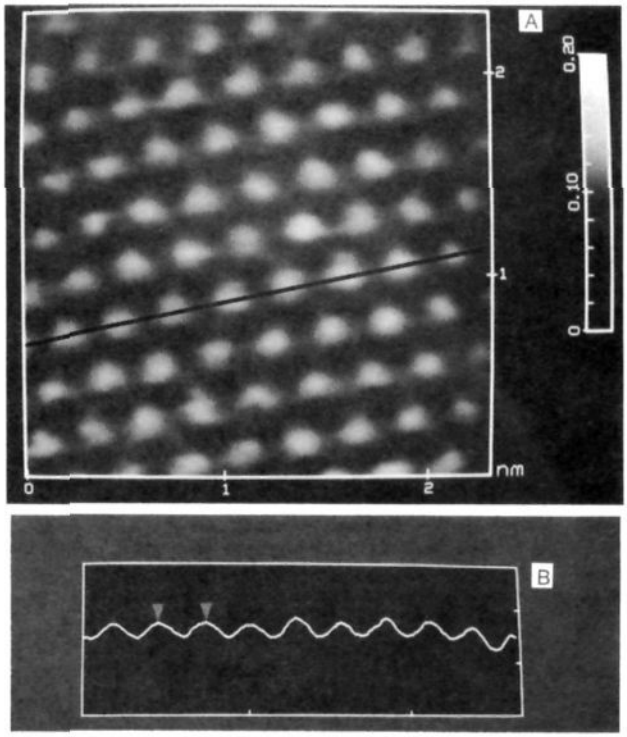

Figure 2. (A) Atomically resolved 2.3 nm × 2.3 nm section of an epitaxially deposited Au film on mica. The image was recorded in the constant height mode using a bias voltage of 100 mV and a tunneling current of 1.5 nA. This image was low-pass filtered. The z scale is 0–0.20 nm. (B) Contour of the surface for the black line that is superimposed on the image in (A). The markers on the contour indicate a nearest-neighbor spacing of 0.29 nm.

topographical contour plot taken along the black line overlaying the image in Figure 2A. The distance between the markers in Figure 2B gives a nearest-neighbor spacing of 0.29 ± 0.02 nm, which compares well with the 0.288-nm interatomic separation of Au atoms[11] of a (111) surface. Larger area scans show that the spacing exists for lateral tip translations of tens of nanometers. When these figures are examined, it is important to note that the vertical corrugation along the contour is a manifestation of the density of states in the electronic band structure at the surface, as opposed to an actual topographical distance.[11]

The predominance of the (111) character of our Au films is consistent with that indicated by the current–potential curves for the underpotential deposition of Pb(II) by linear sweep voltammetry.[3,15] Earlier studies with both low-energy electron diffraction[11] and X-ray diffraction[10] support our conclusion. On the basis of these results, we will refer to our Au substrates simply as Au(111).

3. A. STM Images of Ethanethiolate Monolayers on Au(111). All of the images presented in this section were obtained by using constant height imaging. Also, as noted in the figure captions, several of the images have been smoothed with an eight-point moving average algorithm, i.e., the low-pass filter utility of the Nanoscope II software. The remaining images are not smoothed.

Figure 3 shows STM images found for a spontaneously adsorbed monolayer of ET at Au(111). Figure 3A is an image slightly less than 8 nm × 8 nm. Figure 3B is an expanded view of the middle right portion of Figure 3A and is slightly greater than 2.5 nm × 2.5 nm. In both images, a hexagonal pattern with a spacing markedly different from that of the Au(111) lattice is evident. The spacings of this pattern are given by contour plots in Figure

(13) We have occasionally found complex images that we have not yet been able to interpret. Interestingly, we have not found these complex images with atomic force microscopy; only images comparable to Figures 3 and 5 have been observed. Presently, we do not know what variation in experimental parameters causes these complex images.

(14) Ulman, A.; Eilers, J. E.; Tillman, N. *Langmuir* **1989**, *5*, 1147–1152.

(15) This determination was based on the comparison of the underpotential deposition (UPD) of Pb(II) onto the Au films on mica to published UPD curves on Au single crystal faces (Schultze, J. W.; Dickertman, D. *Surf. Sci.* **1976**, *54*, 489. Engelsman, K.; Lorenz, W. J.; Schmidt, E. *J. Electroanal. Chem.* **1980**, *114*, 1).

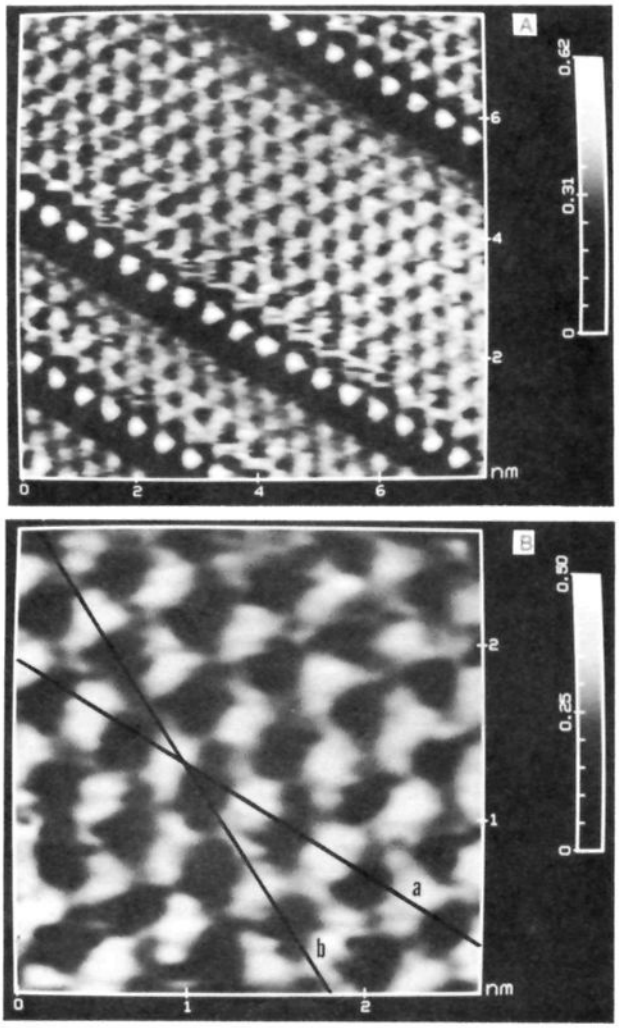

Figure 3. Images of 7.7 nm × 7.7 nm (A) and 2.65 nm × 2.65 nm (B) sections of an ethanethiolate monolayer on an epitaxially grown Au film on mica. (A) Unfiltered; z scale of 0–0.62 nm. (B) Low-pass filtered; z scale of 0–0.50 nm. The images were recorded in a constant height mode using a bias voltage and tunneling current of −200 mV and 2 nA, respectively. (C) Contours of the image along the lines a and b in (B). The markers in the upper contour indicate the nearest-neighbor spacing of 0.51 ± 0.02 nm along line a. The markers in the lower contour indicate the next-nearest-neighbor spacing of 0.91 ± 0.04 nm along line b.

3C, which are taken along the dark lines overlaying the image of Figure 3B. The triangular markers in the upper and lower contours of Figure 3C indicate respective nearest-neighbor and next-nearest-neighbor spacings of 0.51 (±0.02) and 0.91 (±0.04) nm. The uncertainties in the spacings are consistent for all of our ET samples. The average nearest-neighbor and next-nearest-neighbor spacings from more than 20 samples are 0.50 (±0.02) and 0.87 (±0.04) nm, respectively, which are consistent with a $(\sqrt{3} \times \sqrt{3})R30°$ adsorbate layer on a Au(111) surface. Such a two-dimensional arrangement has also been found for long-chain n-alkanethiols adsorbed at Au(111) via helium[1] and electron[2] diffraction studies. Additionally, the spacings in the images are comparable to those found at our OT-coated samples (vida infra) as well as to those found in a few preliminary scans of monolayers from n-decanethiol.

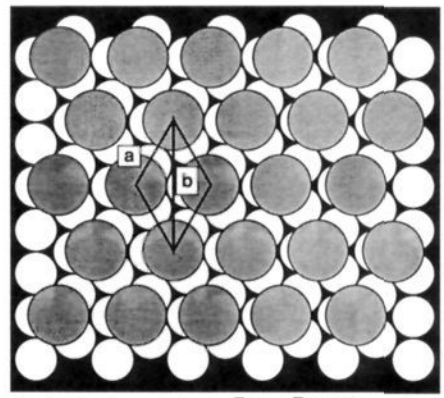

Figure 4. Scale drawing of the $(\sqrt{3} \times \sqrt{3})R30°$ overlayer with the underlying Au(111) surface. The open circles represent the Au atoms, and the shaded circles represent the hydrocarbon chain. The nearest- and next-nearest-neighbor spacings are (a) 0.50 and (b) 0.87 nm, respectively, as marked on the figure (see text for additional details).

For comparison to the image in Figure 3B, Figure 4 provides a scale drawing of a Au(111) surface (open circles) with a commensurate overlayer of adsorbate molecules (shaded circles) representing an n-alkanethiolate monolayer. The packing of the overlayer was determined by assuming that each adsorbate molecule binds at an equivalent site. The 0.42-nm diameter of the overlayer structure equals that for a closest-packed array[14] of alkyl chains. Although our images do not provide information concerning registry with the underlying substrate, we have placed the adsorbates in equivalent threefold hollow sites as previously suggested.[2,9b] An identical overlayer structure may be drawn with n-alkanethiolate molecules centered at either on-top or twofold bridging sites. In all three cases, the respective nearest- and next-nearest-neighbor spacings of the overlayer structure are 0.498 and 0.864 nm, which agree with those of Figure 3B.

In addition to packing information, the large area scan in Figure 3A shows that the hexagonal periodicity extends over an 8 nm × 8 nm region. We have occasionally seen continuous periodicity over much larger areas (~600 nm^2). Such a finding suggests the potential value of STM for probing relationships between macroscopic properties such as wetting[4h,i,6] and the domain size of the monolayers.

Also apparent in Figure 3A are rows of the adsorbate that appear brighter than others. We believe these rows correspond to single atomic steps on the substrate surface, though it is not clear if their "raised" appearance has chemical significance or is an artifact of imaging. For example, binding at edge sites should involve different adsorbate–substrate orbitals, which may be manifested in the images. However, this "brightness" may also occur because electrons can tunnel both vertically and laterally between the tip and substrate as the tip approaches the step edge from the upper surface.

B. STM Images of n-Octadecanethiolate Monolayers on Au(111). Parts A and B of Figure 5 show STM images of an OT-coated Au sample for respective areas of 8.15 nm × 8.15 nm and 2.65 nm × 2.65 nm. As with the ET-coated samples, a hexagonal structure is evident with nearest- and next-nearest-neighbor spacings that are markedly different from that for uncoated Au(111). The spacings of the images, which are outlined in black in Figure 5B, are consistent with the $(\sqrt{3} \times \sqrt{3})R30°$

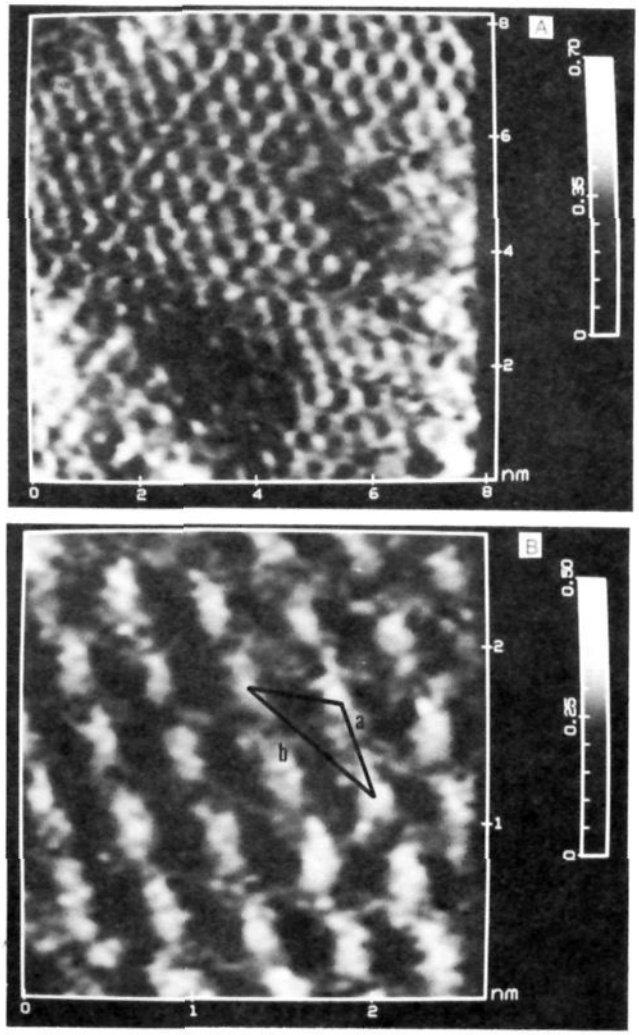

Figure 5. Images of 8.15 nm × 8.15 nm (A) and 2.65 nm × 2.65 nm (B) sections of *n*-octadecanethiolate on an epitaxially grown Au film on mica. Both images were low-pass filtered. The *z* scale is 0–0.70 nm for (A) and 0–0.50 nm for (B). The images were recorded in the constant height mode with a bias voltage of −200 mV and a 2-nA tunneling current. The spacings marked on (B) are (a) 0.50 ± 0.02 and (b) 0.88 ± 0.04 nm.

overlayer found at our ET-coated samples. We also note that the images for the OT monolayers are consistently noisier than those observed for the ET-coated surfaces and that we have not been able to obtain images for the OT overlayers over as large an area as the ET overlayers. Although not understood, we presently attribute both differences to the presence of the longer alkyl chain of OT.

Taken together, the images in Figures 3 and 5 indicate that our monolayers can be successfully characterized at an atomic scale with STM. These results further reveal that the adsorbate adopts a $(\sqrt{3} \times \sqrt{3})R30°$ overlayer arrangement on a Au(111) lattice.

4. Comparison with Structural Descriptions of Thiols on Au from Macroscopic Data. Although our images reveal the two-dimensional arrangement for only an extremely small fractional area of the overlayer, comparisons with structural descriptions developed from "macroscopic" measurements argue that the observed packing is a reasonable representation of the predominant structure at the surface. For example, we have recently discovered that *n*-alkanethiolate monolayers at Au(111) can be desorbed by a one-electron reduction.[3] Integration of the charge for the desorption provides a measure of the adsorbate surface coverage. After accounting for roughness, we found a surface coverage of 8.4 (±0.7) × 10^{-10} mol/cm^2 for all of the thiolate monolayers tested [$CH_3(CH_2)_nSH$, n = 3–18]. This value agrees reasonably well with the theoretical 7.6 × 10^{-10} mol/cm^2 coverage expected for a $(\sqrt{3} \times \sqrt{3})R30°$ overlayer at Au(111). In addition, a closest-packed array of alkyl chains in a $(\sqrt{3} \times \sqrt{3})R30°$ overlayer structure would exhibit a chain tilt of ~35° from the surface normal.[14] Such a tilt is consistent with the 30–40° average tilts determined for long-chain alkanethiol monolayers by an orientational analysis of infrared reflection spectroscopic data.[4d,i] Taken together, the similarities of the structural descriptions provided by these macroscopic measurements and by our STM images suggest that the $(\sqrt{3} \times \sqrt{3})R30°$ overlayer is the predominant two-dimensional arrangement of our *n*-alkanethiolate monolayers at Au(111). To develop this description further, we are beginning experiments to assess the relationship between imperfections in the substrate (e.g., grain boundaries) and structural imperfections in the monolayer.

5. Possible Mechanism for the Imaging of Alkanethiolate Adsorbates. Assumptions concerning the relative position of the microscope tip from the sample surface during imaging influence the structural interpretation of the images. As previously stated, we believe that our images result from electrons tunneling between the tip and the Au-bound sulfur of the alkanethiolate adsorbate. The conclusion is based primarily on the observation that both the coated and uncoated Au samples can be successfully imaged with comparable tunneling currents and bias voltages. This argues that imaging under our experimental conditions is not observably affected by the presence of the hydrocarbon layer, although, as noted, the long-chain images are typically noisier than the short-chain images. As such, we believe that the tip is positioned near the Au–S interface during imaging. Interestingly, recent studies of Langmuir–Blodgett films of cadmium arachidate, phospholipids,[8d,j] and adsorbed detergent layers[8k] have yielded images indicative of the structure of the outer boundaries of the organic film, a separation distance of 3–5 nm between the tip and the substrate. Such large separation distances suggest that a "through-bond" long-range electron-transfer mechanism[16] may also be operative in imaging with STM.[8k] The ability to image both our coated and uncoated Au samples under the same conditions, however, argues that a through-bond mechanism plays a minor role in imaging our monolayers. We are presently assessing the validity of our interpretation through measurements of the heights of the tunneling barriers of the layers and considerations of current theoretical models.[17]

Conclusions

The most significant statement concerning these results herein is that we have found it possible to resolve atomically sized features of monomolecular organic films on gold by STM under ambient conditions. This finding adds to the rapidly growing list of imageable adsorbates and suggests a promising future for the utilization of STM in a number of areas in which detailed information concerning the structure at a metal–adsorbate interface in a non-ultra-high vacuum environment is desired. Our results also complement and enhance the current understanding of the packing arrangement of *n*-alkanethiolate films on gold. We have observed domains of adsorbate surface structure that are well described as $(\sqrt{3} \times \sqrt{3})R30°$ overlayers commensurate with a Au(111) substrate. This is in agreement with structures proposed for *n*-alkanethiolate layers on the basis of the results of helium diffraction[1] and transmission electron diffraction[2] studies. We have also been able to observe continuous domains of this structure for areas as large as 25 nm × 25 nm. Though sampling has not yet been extensive enough to determine if such domain sizes are typical, such an observation suggests the potential value of STM for addressing important questions about the long-range order

(16) (a) Closs, G. L.; Calcaterra, L. T.; Green, N. J.; Penfield, K. W.; Miller, J. R. *J. Phys. Chem.* **1986**, *90*, 3673. (b) Penfield, K. W.; Miller, J. R.; Paddon-Row, M. N.; Cotsaris, E.; Oliver, A. M.; Hush, N. S. *J. Am. Chem. Soc.* **1987**, *109*, 5061.

(17) (a) Tersoff, J.; Hamann, D. R. *Phys. Rev. Lett.* **1983**, *50*, 1998–2001. (b) Tersoff, J.; Hamann, D. R. *Phys. Rev. B* **1985**, *31*, 805–813.

within the adsorbate layer. Experiments are underway to evaluate further the capability to image these and various other hydrocarbon-based monolayers.

Acknowledgment. M.D.P. gratefully acknowledges the support of a Dow Corning Assistant Professorship. Acknowledgment is also made to the donors of the Petroleum Research Fund, administered by the American Chemical Society, for support of this work. Ames Laboratory is operated for the U.S. Department of Energy by Iowa State University under Contract No. W-7405-eng-82. This work was supported by the Office of Basic Energy Sciences, Chemical Science Division.

OPLS Potential Functions for Nucleotide Bases. Relative Association Constants of Hydrogen-Bonded Base Pairs in Chloroform

Julianto Pranata, Scott G. Wierschke, and William L. Jorgensen*

Contribution from the Department of Chemistry, Purdue University, West Lafayette, Indiana 47907. *Received March 5, 1990*

Abstract: Potential functions in the OPLS format have been developed for the nucleotide bases and 2,6-diaminopyridine by fitting to the results of ab initio 6-31G(d) calculations for numerous base–water complexes. These potential functions yield dipole moments and base pair interaction energies in good agreement with available experimental data. The potential functions were tested further in Monte Carlo simulations with statistical perturbation theory to calculate the relative free energies of binding in chloroform for 9-methylguanine with 1-methylcytosine (G–C) versus 9-methyladenine with 1-methyluracil (A–U), and for G–C versus 1-methyluracil with 2,6-diaminopyridine (U–DAP). The calculations predict the G–C complex to be more stable than both the A–U and U–DAP complexes by about 5 kcal/mol. The similar stabilities for complexes like A–U and U–DAP are observed experimentally, though the quantitative enhancement in going to G–C appears to be exaggerated in the simulations. The large difference in association constants between G–C and the similarly triply hydrogen-bonded U–DAP is traced to the gas-phase interaction energies, which favors G–C by about 10 kcal/mol. This in turn is caused by the different arrangement of hydrogen bond donor and acceptor sites in the two complexes, which leads to secondary electrostatic interactions that disfavor U–DAP relative to G–C. The general importance of such secondary interactions for understanding variations in association is discussed.

Introduction

The interaction between nucleotide bases is an important element in the structure of DNA. Consequently, there have been numerous studies, experimental[1-8] and computational,[9-16] concerned with the association of nucleotide base pairs. The computational studies range from gas-phase energy minimizations[9-12] to Monte Carlo and molecular dynamics simulations in solution.[13-16] The work of Pohorille, Kollman, and co-workers is particularly notable.[15,16] Pohorille et al. performed seminal Monte Carlo simulations of stacked and hydrogen-bonded base pairs in CCl_4 and in water.[15] However, only the interaction energies (ΔE's) were calculated, while the more relevant measure of association is the free energy, ΔG. The bases were not allowed to move relative to one another, and the interaction energies were calculated by computing the differences in the total energies for the complex in solution and for the individual bases. This involves computing a small difference between large fluctuating numbers which leads to difficulties with precision. Subsequently, Cieplak and Kollman carried out molecular dynamics calculations for the A–T and G–C base pairs in vacuo and in water.[16a] Free energy changes were now calculated using statistical perturbation theory. The calculations featured arduous series of simulations in which each base and the complexes were made to vanish in water. It was correctly predicted that stacked structures were more stable than hydrogen-bonded ones in water, though the nature of the perturbations and simulation times led to significant uncertainties for the free energy changes.

Recently, Dang and Kollman calculated the free energy of association of 9-methyladenine and 1-methylthymine in water using a different approach.[16b] In this case the potential of mean force (PMF) of the base pair was obtained from a series of simulations in which the bases were gradually perturbed apart. Calculation of the association constant, K_a, then involves an integration of the PMF to a cutoff value that defines association.[17] The relative orientation of the bases was forced to remain constant as they were separated. Though the preference for stacking

* Address correspondence to this author at the Department of Chemistry, Yale University, New Haven, CT 06511.

(1) Kyogoku, Y.; Lord, R. C.; Rich, A. *Proc. Natl. Acad. Sci. U.S.A.* **1967**, *57*, 250.
(2) Kyogoku, Y.; Lord, R. C.; Rich, A. *Biochim. Biophys. Acta* **1969**, 179, 10.
(3) Iwahashi, H.; Kyogoku, Y. *J. Am. Chem. Soc.* **1977**, *99*, 7761. Watanabe, M.; Sugeta, H.; Iwahashi, H.; Kyogoku, Y.; Kainosho, M. *Eur. J. Biochem.* **1981**, *117*, 553. Iwahashi, H.; Sugeta, H.; Kyogoku, Y.; *Biochemistry* **1982**, *21*, 631.
(4) Newmark, R. A.; Cantor, C. R. *J. Am. Chem. Soc.* **1968**, *90*, 5010.
(5) Petersen, S. B.; Led, J. J. *J. Am. Chem. Soc.* **1981**, *103*, 5308.
(6) Williams, L. D.; Chawla, B.; Shaw, B. R. *Biopolymers* **1987**, *26*, 591.
(7) Williams, N. G.; Williams, L. D.; Shaw, B. R. *J. Am. Chem. Soc.* **1989**, *111*, 7208.
(8) Yanson, I. K.; Teplitsky, A. B.; Sukhodub, L. F. *Biopolymers* **1979**, *18*, 1149.
(9) Pullman, B.; Claverie, P.; Caillet, J. *Proc. Natl. Acad. Sci. U.S.A.* **1966**, *55*, 904.
(10) (a) Kudritskaya, Z. G.; Danilov, V. I. *J. Theor. Biol.* **1976**, *59*, 303. (b) Langlet, J.; Claverie, P.; Caron, F.; Boeuve, J. C. *Int. J. Quantum Chem.* **1981**, *19*, 299.
(11) Hobza, P.; Sandorfy, C. *J. Am. Chem. Soc.* **1987**, *109*, 1302.
(12) Aida, M. *J. Comput. Chem.* **1988**, *9*, 362.
(13) Danilov, V. I.; Tolokh, I. S.; Poltev, V. I.; Malenkov, G. G. *FEBS Lett.* **1984**, *167*, 245. Danilov, V. I.; Tolokh, I. S.; Poltev, V. I. *FEBS Lett.* **1984**, *171*, 325. Danilov, V. I.; Tolokh, I. S. *FEBS Lett.* **1984**, *173*, 347.
(14) Egan, J. T.; Nir, S.; Rein, R.; MacElroy, R. *Int. J. Quantum Chem. Quantum Biol. Symp.* **1978**, *5*, 433.
(15) Pohorille, A.; Pratt, L. R.; Burt, S. K.; MacElroy, R. D. *J. Biomol. Struct. Dyn.* **1984**, *1*, 1257. Pohorille, A.; Burt, S. K.; MacElroy, R. D. *J. Am. Chem. Soc.* **1984**, *106*, 402.
(16) (a) Cieplak, P.; Kollman, P. A. *J. Am. Chem. Soc.* **1988**, *110*, 3734. (b) Dang, L. X.; Kollman, P. A. *J. Am. Chem. Soc.* **1990**, *112*, 503.
(17) Jorgensen, W. L. *J. Am. Chem. Soc.* **1989**, *111*, 3990.

0002-7863/91/1513-2810$02.50/0